New Phytologist

Research

Root tip excision-induced exodermis lignification impacts lateral root emergence in *Brachypodium distachyon*

Kevin Bellande[1,2], Cristovão De Jesus Vieira Teixeira[1], Marius Malai[1], Angelina D'Orlando[3], Léa Perez[3], Richard Sibout[3], Anne C. Roulin[4], Joop E. M. Vermeer[1] and Thomas Badet[1]

[1]Laboratory of Molecular and Cellular Biology, Institute of Biology, University of Neuchâtel, Rue Emile Argand 11, CH-2000, Neuchâtel, Switzerland; [2]IPSiM, University of Montpellier, CNRS, INRAE, Institut Agro, 34000, Montpellier, France; [3]INRAE, UR 1268 BIA, 44316, Nantes, France; [4]Agroscope, 8820, Wädenswil, Switzerland

Authors for correspondence:
Kevin Bellande
Email: kevin.bellande@cnrs.fr

Joop E. M. Vermeer
Email: joop.vermeer@unine.ch

Thomas Badet
Email: thomas.badet@unine.ch

Received: *2 September 2025*
Accepted: *10 December 2025*

New Phytologist (2026)
doi: 10.1111/nph.70883

Key words: *Brachypodium distachyon*, comparative transcriptomics, lateral root formation, lignification, response to stress, root system architecture diversity.

Summary

- The mechanisms controlling lateral root emergence in monocots, particularly the role of the exodermis, are poorly understood. We investigated how natural variation in the *Brachypodium distachyon* stress response shapes root system architecture by modulating cell wall dynamics.
- We used root tip excision to synchronize lateral root development across natural accessions. The resulting phenotypes were analysed using comparative transcriptomics, biochemical lignin quantification, confocal Raman spectroscopy, and chemical inhibition of lignin biosynthesis.
- Two distinct root system architectures, 'pine tree' and 'fishbone', were identified. The 'fishbone' phenotype results from an altered lateral emergence caused by a differential lignification intensity of the exodermis. This phenotype was accompanied by the transcriptional upregulation of lignin biosynthesis genes and was partially rescued by treatment with a lignin inhibitor.
- Stress-induced exodermal lignification acts as a mechanical 'brake' on lateral root emergence. This positions the exodermis as a key regulatory hub that integrates environmental cues with lateral root development to control Root System Architecture plasticity in grasses.

Introduction

Plants exhibit remarkable intraspecific phenotypic variation, enabling individuals within a species to respond and adapt to diverse environmental conditions. In plants, natural variation has been extensively characterized for aboveground traits such as flowering time and abiotic stresses (Filiz *et al.*, 2009; Schwartz *et al.*, 2010; Luo *et al.*, 2011; Ingram *et al.*, 2012; González *et al.*, 2020; Stritt *et al.*, 2022; Ludwig *et al.*, 2024). Increasing evidence also points to substantial variation in belowground traits, particularly root system architecture (Chochois *et al.*, 2015; Rouina *et al.*, 2025). Indeed, root system architecture plasticity is a key component of plant adaptation to changing environmental conditions, enabling dynamic modulation of water and nutrient foraging strategies (Lynch *et al.*, 1995; Smith & de Smet, 2012; Maqbool *et al.*, 2022). A central mechanism driving root plasticity is the formation of lateral roots, which remodel the root system in response to developmental and environmental cues (Lynch, 2019; Ramachandran *et al.*, 2024).

Lateral root development requires coordinated cellular processes such as cell division, expansion, and differentiation, which occur within the context of a mechanically complex tissue (Beckers *et al.*, 2024). To emerge, lateral root must traverse several established cell layers of the primary root, posing significant physical constraints (Stoeckle *et al.*, 2018; Vadodaria & Anderson, 2025). These constraints are mediated by plant cell walls, which are composed of polysaccharide polymers such as cellulose, hemicellulose, and pectin (in dicot primary cell walls), and often reinforced with lignin, particularly in secondary cell walls of differentiated tissues such as the endodermis and exodermis (Sarkar *et al.*, 2009; Geldner, 2013; Voxeur *et al.*, 2015; Höfte & Voxeur, 2017; Artur *et al.*, 2021; Liu & Kreszies, 2023). While these cell layers serve as structural barriers and diffusion regulators, they must also undergo regulated remodelling to allow lateral root emergence (Shang *et al.*, 2025; Vadodaria & Anderson, 2025).

In *Arabidopsis thaliana*, the molecular pathways controlling cell wall remodelling during lateral root initiation from xylem pole pericycle cells are well-established (Swarup *et al.*, 2008; Péret *et al.*, 2012; Kumpf *et al.*, 2013; Lewis *et al.*, 2013; Lucas *et al.*, 2013; Roycewicz & Malamy, 2014; Vermeer *et al.*, 2014; Berhin *et al.*, 2019; Wachsman *et al.*, 2020; Ursache *et al.*, 2021). However, the regulation and evolutionary variability

of these mechanisms in monocots, which possess distinct root anatomies, remain poorly understood (Petrova *et al.*, 2023; Zhu *et al.*, 2025). In *Brachypodium distachyon*, lateral root formation involves not only the pericycle but also contributions from the endodermis and cortex (De Jesus Vieira Teixeira *et al.*, 2024). To emerge, lateral roots must ultimately overcome the exodermis, a suberin- and lignin-rich outer barrier whose role during organogenesis remains unclear (Liu & Kreszies, 2023). The composition and mechanical properties of the exodermis, particularly its lignification patterns, vary across species and are likely to influence lateral root development (Voxeur *et al.*, 2015; Cantó-Pastor *et al.*, 2024; Manzano *et al.*, 2024).

Here, we propose that the exodermis functions not only as a diffusion barrier but also as a regulatory interface that integrates stress signals to modulate root branching. We use root tip excision to synchronize lateral root development and uncover natural variation in root system architecture between two *B. distachyon* accessions: Bd21 and Bd21-3. Through comparative transcriptomics, cell wall profiling, and microscopy, we demonstrate that these phenotypic differences are driven by distinct cell wall remodelling processes, with differential stress-induced lignification of the exodermis emerging as a primary determinant of emergence.

Materials and Methods

Plant materials and growth conditions

A total of 23 *Brachypodium distachyon* (L.) P.Beauv. accessions were used in this study: Bd21, Bd21-3, SAP47, CM3, BdtR7a, TEK2, GES1, BdTR8C, ko21, Adi2, BdTRIIA, BdTRIIG, BdTR10C, Fo21, BdTR9K, GAZ8, ABR7, PER4, Lam13, Bd30-1, RON2, CRO24, and SAN11, as previously described (Stritt *et al.*, 2022). Seeds were dehulled and surface-sterilized in 6% (v/v) bleach containing 0.01% Triton™ X-100 (Ref: X100-5ML; Sigma-Aldrich) for 1 min, then rinsed six times with sterile water. Sterilized seeds were sown on square 12 × 12 cm Petri dishes containing 1% plant agar (w/v) supplemented with half-strength Murashige and Skoog (½ MS) basal medium and buffered with 2-Morpholinoethanesulfonic acid monohydrate (MES) Buffer. No > 15 seeds were placed in a single row *c.* 3.5 cm from the top edge of each plate, with embryos facing upwards and avoiding direct contact with the medium surface. Plates were placed vertically at an angle of *c.* 20° in growth chambers under continuous light at 22°C to promote root growth along the surface. For root tip excision experiments, 6-d-old seedlings had *c.* 0.5 cm of the primary root tip removed using a sterile scalpel. After excision, plates were resealed and returned to the same growth conditions to allow for synchronized lateral root formation. Samples for RNA-sequencing were collected at 0, 1, 2, 4, 8, and 12 h following root tip excision. For each time point, a 5-mm segment of the root, immediately proximal to the cut, was harvested from a pool of 20–30 seedlings. All samples were immediately flash-frozen in liquid nitrogen upon collection. For chemical inhibition of lignin biosynthesis, 6-d-old seedlings were grown on ½ MS 1% agar plates. After the root tip excision, a sterile filter paper saturated with a mock solution (liquid ½ MS basal medium solution) or a 10 μM solution of piperonylic acid (PA) was gently applied to the whole root system. Treated seedlings of both Bd21 and Bd21-3 accessions were maintained under growth chamber conditions for 60 h before phenotypic observation and quantification of lateral root numbers.

RNA extraction, library preparation, and sequencing

For the *B. distachyon* Bd21 and Bd21-3 accessions, total RNA was extracted from root tips after excision using the SV Total RNA Isolation System (Promega) according to the manufacturer's instructions. The RNA samples were shipped to Novogene (NOVOGENE (UK) Co. Ltd) for quality control, library preparation, and high-throughput sequencing. RNA integrity and purity were first assessed by Novogene's in-house quality control pipeline, and only samples with sufficient RNA integrity number and concentration passed to library preparation. Messenger RNA was enriched from total RNA using poly-T oligo-attached magnetic beads, followed by fragmentation and first-strand cDNA synthesis with random hexamer primers. Second-strand cDNA synthesis, end-repair, A-tailing, adapter ligation, and PCR enrichment were performed to generate sequencing-ready libraries. Libraries were prepared as unstranded, paired-end libraries, and sequenced on an Illumina NovaSeq 6000 platform, yielding 150 base-pair paired-end reads (PE150). Approximately 6 Gb of raw sequencing data per sample was generated, with > 85% of bases expected to reach Q30 quality standards. The generated raw reads were first filtered for polyA and TruSeq adapters using the BBduck tool from the BBMap suite (v.38.96) (options ref = polyA.fa.gz,truseq.fa.gz ktrim = r k = 23 mink = 11 hdist = 1 tpe tbo qtrim = r trimq = 10 minlength = 20) (Bushnell *et al.*, 2014). The resulting trimmed reads were next aligned to the respective genome assembly (BdistachyonBd21_3_537_v1.0 for Bd21-3, and Bdistachyon_314_v3 for Bd21) using STAR aligner (v.2.7.10a) (Dobin *et al.*, 2013). The genome index was built using strings of 12 bases (--genomeSAindexNbases 12), and reads were aligned allowing for multiple matches (options --outFilterMultimapNmax 100 --winAnchorMultimapNmax 200) (Li *et al.*, 2009). The coordinate-sorted BAM files were indexed with SAMTOOLS (v.1.15.1), and read counts were calculated using the union method implemented by the htseq-count tool from the HTSeq suite (v.2.0.2) using v.1.2 of the Bd21-3 genome annotation (BdistachyonBd21_3_537_v1.2.gene.gff3) (Anders *et al.*, 2015).

Pangenome reconstruction

To identify homologs between the annotated genes in Bd21 and Bd21-3 accessions, we first extracted all coding sequences given the gene annotations using GFFREAD v.0.12.7 (BdistachyonBd21_3_537_v1.2 and Bdistachyon_556_v3.2 available at the Phytozome v.14 database) (Pertea & Pertea, 2020). The transcripts were translated into proteins using the *transeq* tool from the EMBOSS:6.6.0.0 suite, and orthology between Bd21 and Bd21-3 proteins was finally inferred using ORTHOFINDER v.2.5.5 with default parameters (-og -a 12) (Rice *et al.*, 2000; Emms & Kelly, 2019).

Differential expression analysis

Differential expression analysis was performed using R v.4.1.2 and the DESEQ2 package v.1.32.0 ('R: The R Project for Statistical Computing', n.d.; Love *et al.*, 2014). Genes with null expression in > 20% of the samples were filtered out. The data dispersion was estimated using the *vst* function implemented in DESeq2 package using a sample of 20 000 genes (nsub = 20 000). Differential expression across time points was calculated on genes expressed in at least 20% of the samples and with a total read count ≥ 10. We used the likelihood ratio test to estimate changes in gene expression across the kinetic and extracted results for each comparison using the Wald test implemented in DESEQ2.

Gene ontology enrichments

All Gene Ontology (GO) enrichment analyses were performed using the R package TOPGO v.2.44.0 based on the Bd21 and Bd21-3 annotations (Bdistachyon_556_v3.2.annotation_info.txt and BdistachyonBd21_3_537_v1.2.annotation_info.txt) available on PHYTOZOME v.14 database. Results are shown at the biological processes (BPs) level at a false discovery rate of 5% for GOs annotated in > 10 genes and with > 5 occurrences in the test gene set. Enrichment values are expressed as the number of occurrences of the GO in the test gene set over its Fisher test expected number.

Preparation of hand-sectioned root samples

For sectioning, roots from 6-d-old seedlings of similar length were placed in parallel. Fragments of 1 cm containing the region of interest were partitioned and embedded in 4% agarose. Once solidified, the agarose blocks were glued onto a hand microtome, and sections of *c.* 50 μm were prepared for clearing or immediate visualization. Representative images were obtained from at least 30 seedlings from three independent replicates.

Clearing and staining

Clearing steps using DEEP-Clear were performed as described previously (Pende *et al.*, 2020; De Jesus Vieira Teixeira *et al.*, 2024). The DEEP-Clear solution consists of 5–8% (v/v) THEED, 5% (v/v) Triton X-100, and 25% (w/v) urea in water. Seven-day-old root seedlings were collected and fixed for 1 h in 4% (w/v) paraformaldehyde in 1× phosphate-buffered saline (PBS) with three rounds of soft vacuum infiltration. After fixation, roots were washed five times in 1× PBS. Samples were then transferred to the DEEP-Clear solution and incubated at room temperature with gentle shaking for 7–10 d, with the solution being replaced twice. For staining, stock solutions (1%) of Basic Fuchsin (lignin), Renaissance, and/or Calcofluor (cell wall) were prepared directly in DEEP-Clear. To combine multiple dyes, samples were incubated first in Basic Fuchsin (0.1% in DEEP-Clear) for 1 h and washed overnight. Samples were then transferred to Renaissance (0.1% in DEEP-Clear) for 2 d. To visualize lignified tissues, *B. distachyon* root segments were stained with freshly prepared Wiesner stain (phloroglucinol-HCl). The staining solution was made by dissolving 0.3 g of phloroglucinol in 10 ml of 100% ethanol and then mixing this solution with concentrated HCl at a 2 : 1 (v/v) ratio. Root sections were incubated in the stain for *c.* 10 min at room temperature. The stained sections were immediately mounted on a microscope slide in a drop of the staining solution and observed with a Leica DM4 upright microscope. Due to the transient nature of the stain, images were captured within 10 min of application to prevent signal deterioration. For imaging of Basic Fuchin stained lignin, samples were mounted on microscope slides and imaged either on a Leica SP8-DIVE multiphoton confocal microscope using the settings described by De Jesus Vieira Teixeira *et al.* (2024) or on a Leica Stellaris WLLplus confocal microscope. For the latter, 557 nm was used for excitation and fluorescence was collected between 565 and 650nm.

Quantification of lignin

For the cysteine-assisted sulfuric acid (CASA) lignin method, three independent replicates were prepared for Bd21 and for Bd21-3. Thirty whole roots were collected (10 seedlings per replicate in three square dishes), pooled, frozen in liquid nitrogen, and ground for 2 min at full speed. The samples were then dried in 2-ml Eppendorf tubes at 40°C for 24 h. A cysteine stock solution (0.1 g ml^{-1}) in 72% sulfuric acid (SA) was prepared by dissolving 10 g L-cysteine in 100 ml SA. The solvent-extracted biomass sample (*c.* 5 mg) was placed in a 4-ml glass vial, and 1.0 ml of the cysteine stock solution was added. The mixture was sealed with a Teflon-lined screw cap and stirred at 24°C (500 rpm) for 60 min until complete biomass dissolution. The solution was then diluted 1/50 by adding 20 μl of the solution to 980 μl of deionized water in a 4-ml vial. The absorbance at 283 nm (A_{283}) was measured using a UV spectrophotometer against a blank. If necessary, a UV absorption spectrum was recorded from 230 to 400 nm at 1-nm intervals. Lignin content (CASA_L%) was calculated using the Beer–Lambert law. All tests were performed in triplicate, and data are presented as mean ± SD.

For the thioacidolysis, root segments from 30 to 50 individual roots were collected from two distinct regions: a proximal region (5 mm above the apex after root tip excision) and an upper region (from 5 mm above the apex to the root collar). Samples were pooled, weighed, and lyophilized. The thioacidolysis reagent was prepared by mixing 2.5 ml BF_3 etherate (Aldrich) and 10 ml ethane thiol (EtSH, Aldrich) in a 100-ml flask, adjusting the final volume to 100 ml with dioxane (pestipur grade). The extract-free biomass (*c.* 5 mg) was incubated with 3 ml of reagent and 0.1 ml of an internal standard solution (2.5 mg ml^{-1} heneicosane in CH_2Cl_2) in a Teflon-lined screw-capped glass tube. Thioacidolysis was conducted at 100°C for 4 h. After cooling, the pH of the reaction mixture was adjusted using 0.2 M $NaHCO_3$, followed by the addition of 0.1 ml of 6 M HCl. The mixture was extracted with 2 ml of CH_2Cl_2, and after phase separation, the lower organic phase was recovered and dried over Na_2SO_4. The solvent was evaporated under reduced pressure at 40°C until *c.* 0.5 cm of liquid remained in the vial before silylation for GC or GC-MS analysis. Lignin-derived dimers were quantified after desulfurization, and monomer analysis was performed as described (Lapierre & Rolando, 1988).

Confocal Raman spectroscopy

For the sample preparation and spectral acquisition, reference peaks for major cell wall components (e.g. cellulose, hemicellulose, and lignin) were identified by comparison to established literature spectra (Diehn *et al.*, 2024). For the analysis, 7-d-old *B. distachyon* seedlings (accessions Bd21 and Bd21-3) were grown *in vitro* and sampled at 0 and 40 h after root tip excision. Root segments from phenotypically distinct upper root regions were excised, aligned, and embedded in 8% agarose. Transverse sections of 50 µm were obtained using a vibratome (HM 650V; Microm Microtech), air-dried for 10 min, and mounted on Raman slides. Spectra were acquired using a confocal Raman microscope (inVia Reflex, Renishaw) with a 785-nm laser. The system was equipped with a double-edge filter (Rayleigh cutoff at 100 cm^{-1}) and two diffraction gratings (1800 and 1200 l mm^{-1}) for spectral acquisition. An automated XYZ stage allowed for precise 100-nm step displacements. Laser power was optimized to prevent sample damage. Spectra were collected with a resolution of < 4 cm^{-1} and a precision of < 0.5 cm^{-1}. Measurements were focussed on the anticlinal cell walls of the exodermis, with at least 15 root sections analysed from five independent roots per genotype, across three to five biological replicates. Raman measurements were taken in the upper root region where the lateral root emergence delay is observed, focussing on the anticlinal cell walls of the exodermis. All samples were collected 40 h after root tip excision, and for each accession, we specifically measured the exodermal anticlinal cell wall located on the primordium-facing side. Raw spectral data quality was first enhanced by applying cosmic ray removal using the WiRE 4.2 software (Renishaw). Subsequent preprocessing was conducted in OriginLab Pro, which included baseline correction and normalization of the spectra to ensure comparability. Following these steps, an average Raman spectrum was generated for each sample for further analysis. All downstream statistical analyses and data visualization were performed in R (v.4.4.2) utilizing the tidyverse suite of packages. To handle technical duplicates, spectra from replicate measurements for each sample were averaged at each wavenumber. To ensure comparability, only spectra covering the full range from 300 to 1800 cm^{-1} were included in the final analysis. To identify statistically significant differences in cell wall composition between the Bd21 and Bd21-3 accessions, the mean intensity of major cell wall-related peaks was compared for each tissue type using an independent two-sample t-test. A difference was considered statistically significant at $P < 0.05$.

Results

Differential lateral root emergence dynamics in response to primary root tip excision

To explore potential natural variation in lateral root emergence in *B. distachyon*, we employed a root tip excision assay, a method previously shown to synchronize lateral root formation (Pacheco-Villalobos *et al.*, 2013). Focussing on a set of 23 natural accessions spanning the species distribution along the Mediterranean range, the approach revealed two distinct root system architecture phenotypes in response to root tip excision. The reference accession Bd21 together with seven other accessions displayed a 'pine tree' phenotype, characterized by uniformly spaced lateral roots along the primary root axis 4 d after excision (BdTR8i, Tek-2, Sap47, Ges1, BdTR11A, BdTR11G, and Gaz-8). By contrast, Bd21-3 and 14 other accessions exhibited a 'fishbone' phenotype, with lateral roots clustered near the excision site but largely absent in the more upper regions of the primary root (Figs 1a, S1). The two phenotypes segregated in the A-Italia, A-East, and B-East genetic and geographical clusters while accessions from the B-West and C-Italia clusters all displayed the 'fishbone' phenotype (Fig. 1b; Table S1) (Stritt *et al.*, 2022). Altogether, these results show that different responses to root tip excision segregate in natural *B. distachyon* populations.

To determine whether the 'fishbone' or the 'pine tree' phenotypes reflected a constitutive developmental program or rather a specific response to root tip excision, we first compared the root system architecture of two representative accessions under control (nonexcised) conditions. In control conditions without root tip excision, Bd21 and Bd21-3 show similar overall growth and root architecture (Fig. S1). Nonexcised 6-d-old Bd21 accession (pine tree) seedlings developed significantly longer primary roots and a higher number of total lateral roots than Bd21-3 (fishbone) (Fig. 1c). Lateral root density was similar between the two accessions, indicating that the greater number of lateral roots in Bd21 is likely due to its longer primary roots rather than a higher branching frequency (Fig. 1c; Table S2). We next analysed the spatial distribution of emerged lateral roots along the primary root axis of Bd21 and Bd21-3 plants after root tip excision. In both accessions, lateral roots were initiated close to the excision site, and within the 1st centimetre of the root axis, their development appeared comparable. However, beyond 2 cm from the excision point, Bd21-3 exhibited markedly fewer emerged lateral roots. In Bd21, primary root tip excision resulted in consistent lateral root emergence along the root axis, with density gradually declining only near the root–shoot junction. By contrast, in Bd21-3 at 72 h after root tip excision, lateral roots in the upper part of the primary root either failed to emerge or failed to grow into the nutrient medium (Fig. 1d; Table S3). To gain further insights into this difference in lateral root emergence, we followed the temporal progression of lateral root development after the root tip excision over a 32-hour time course (1 mm, 2 mm, and 3 mm above the excision site) (De Jesus Vieira Teixeira *et al.*, 2024). Both Bd21 and Bd21-3 displayed synchronized lateral root development, with early stages detectable 2 h post excision (Stages 1–2) and nearly all primordia reaching late developmental stages by 24 h (Stages 9–10) (Fig. S2; Table S4).

To directly address whether the 'fishbone' phenotype in Bd21-3 results from an altered lateral root emergence, we quantified the number of emerged and nonemerged lateral roots 72 h after root tip excision in the primary root of both accessions. We find that Bd21-3 exhibited a significantly higher proportion of nonemerged lateral roots in the upper region compared with Bd21 (Figs 1e, S3; Table S5). These results indicate that lateral root initiation and development are not impaired in Bd21-3,

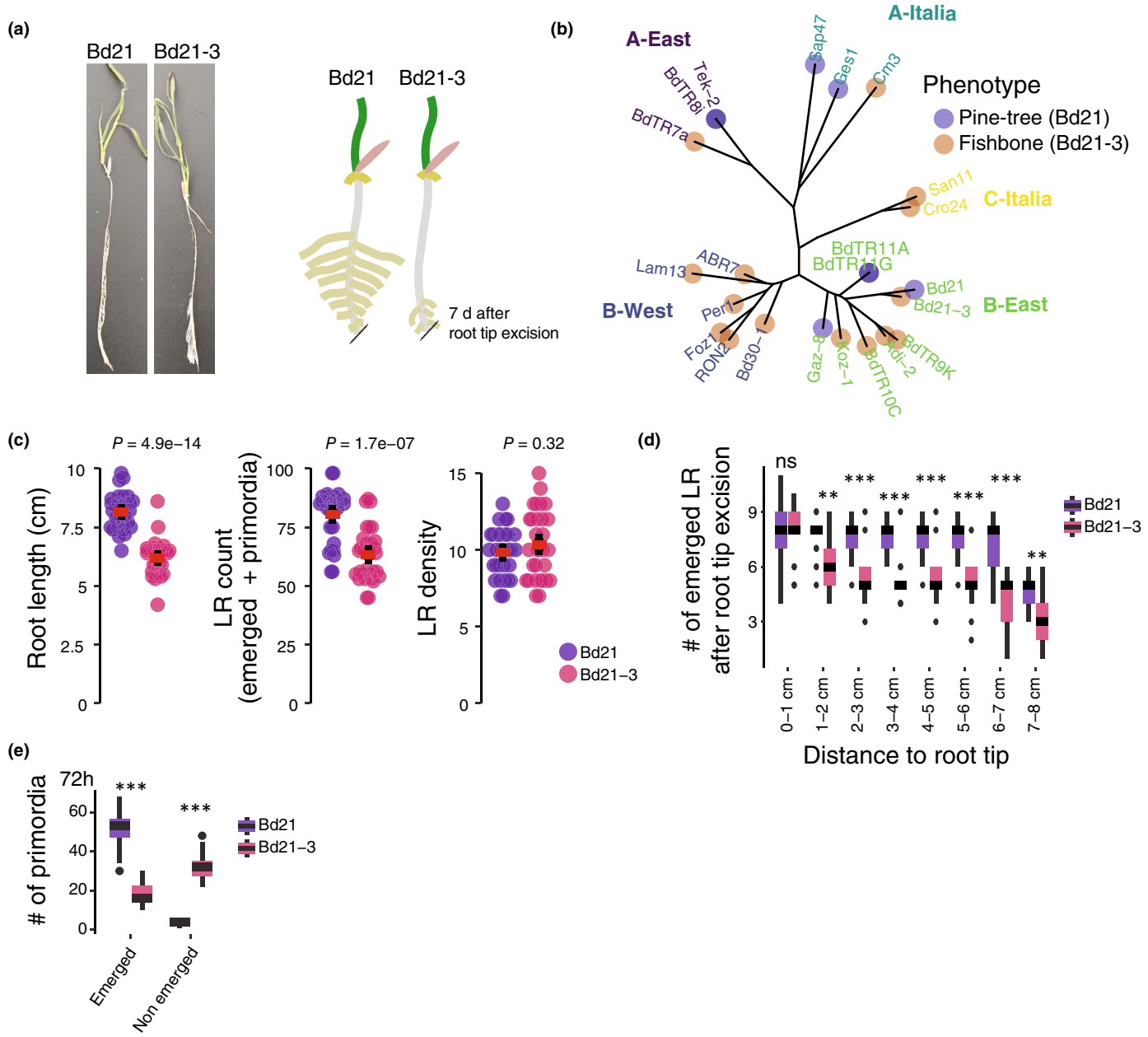

Fig. 1 Bd21 and Bd21-3 display distinct lateral root emergence dynamics following root tip excision. (a) Representative images of *Brachypodium distachyon* accessions Bd21 and Bd21-3 phenotypes and related schematic, 6 d after root tip excision. (b) Geographically structured distribution of the 'pine tree' and 'fishbone' root system architecture phenotypes across a panel of 23 natural *B. distachyon* accessions, indicated geographical clusters (colour codes on the tree). (c) Quantification of root system architecture traits under nonexcised conditions. From left to right: primary root length, total LR count and LR density. (d) Spatial distribution of emerged lateral roots along the primary root axis after root tip excision. (e) Quantification of emerged vs nonemerged lateral root primordia in Bd21 and Bd21-3. Red lines represent the mean values and error bars the SD. For the boxplots, the central boxes represent the interquartile range, spanning the 25th (Q1) to the 75th percentile (Q3). The horizontal line inside each box indicates the median (50th percentile). Whiskers extend to the 5th and 95th percentiles, and individual points outside this range are shown as outliers. Asterisks indicate statistical significance based on a Student's *t*-test (*,$P < 0.05$; **,$P < 0.01$; ***,$P < 0.001$; ns, non significant).

confirming that the observed difference lies in lateral root emergence. Results from nonexcised roots further support the notion that the 'fishbone' phenotype observed in Bd21-3 is not intrinsic but rather arises from a specific phenotypic divergence in the program of lateral root emergence that is triggered or exacerbated by root tip excision.

Comparative transcriptomic analysis reveals extensive cell wall remodelling following root tip excision

To investigate the genetic basis underlying the difference between the 'pine tree' and the 'fishbone' lateral root phenotypes, we first performed a comparative genomic analysis using Bd21 and

New Phytologist

Bd21-3 fully annotated genomes. We assigned the full set of 103 438 proteins to 38 403 ortholog groups (orthogroups), from which *c.* 73% are single-copy orthogroups present in both accessions (28 276/38 403; Fig. 2a; Table S6). The Bd21-3 accession has 3963 orthogroups for which we could not find an ortholog in Bd21. Conversely, 1814 orthogroups are exclusively

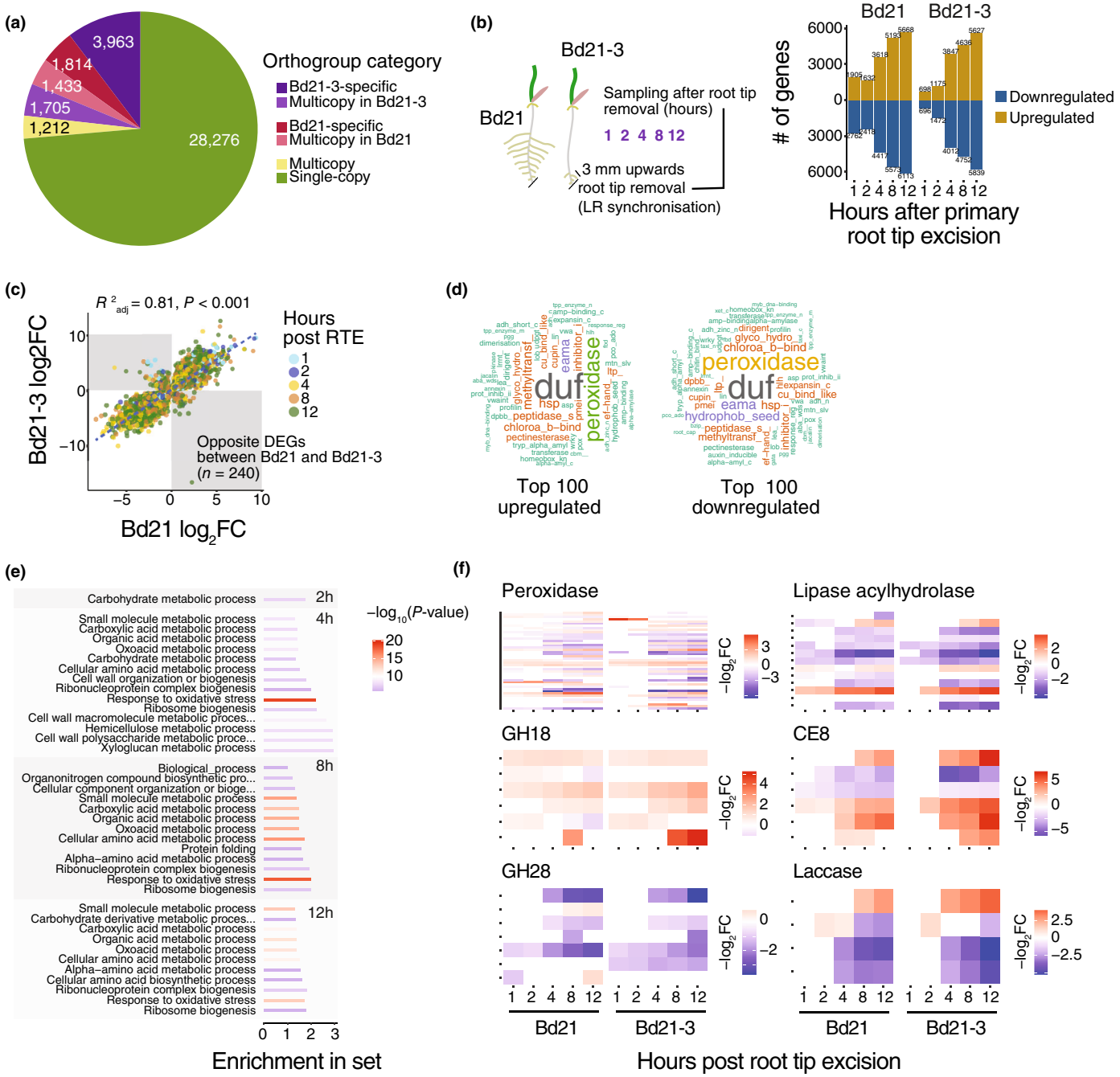

Fig. 2 Comparative genomic and transcriptomic analysis reveals a divergent cell wall remodelling response in Bd21 and Bd21-3 after root tip excision. (a) Pie chart showing the pangenome composition of Bd21 and Bd21-3, with colours indicating the distribution of orthogroup categories. (b) Schematic representation of the time-course transcriptomic experiment following root tip excision for lateral root primordia synchronization (left panel), and the corresponding number of significantly up- and downregulated genes at 1, 2, 4, 8, and 12 h post excision in both accessions (right panel). (c) Correlation plot of $\log_2$ fold-change ($\log_2$FC) values for differentially expressed single-copy orthologs between Bd21 and Bd21-3. Points are coloured by time point postexcision, with a subset of genes showing opposite regulation (shaded boxes). (d) Word clouds representing the most frequent annotation terms among the top 100 upregulated and top 100 downregulated genes across all time points. (e) Gene Ontology enrichment analysis of the biological processes similarly differentially expressed genes (DEGs) at 2, 4, 8, and 12 h after root tip excision compared to 0 h in both accessions. The colour scale indicates the $-\log_{10}$(*P*-value) of Fisher's exact test. (f) Heatmaps showing the fold-change value of DEGs over time for selected cell wall-related enzyme families in both accessions ($-\log_2$FC).

found in the Bd21 accession. A total of 3138 orthogroups have a single protein representative in one of the two accessions while the other has additional proteins attached to the same orthogroup, suggesting recent duplication events in both accessions (Fig. 2a). Orthogroups for which multiple proteins are found in Bd21 but only one in Bd21-3 are enriched for functions related to DNA repair and stress response and might contribute to the phenotypic difference we observe after primary root tip excision (Fig. S4). Thus, the two-accession pangenome reveals substantial gene content variation in *B. distachyon*.

To identify the cellular processes involved in the 'pine tree' and 'fishbone' lateral root phenotypes, we next performed a time-course transcriptomic analysis of the root tissue (at 0; 1; 2; 4; 8; 12 h) after root tip excision in Bd21 and Bd21-3 accessions (Fig. 2b). Approximately 44% and 35% of the annotated genes in Bd21 and Bd21-3, respectively, showed expression in the root tissue in at least one time point (with > 10 read counts). Principal component analysis revealed two major transcriptomic clusters corresponding to early (0–2 h) and late time points (4–12 h) after synchronization (Fig. S5). Compared with Time 0 after synchronization, differential gene expression became more pronounced at the later time points. The number of up- and downregulated genes progressively increased over time, reaching between 3618 and 6113 differentially expressed genes (DEGs) between 4 and 12 h after synchronization (Fig. 2b) (Table S7). At all time points, Bd21 exhibited more DEGs than Bd21-3, likely reflecting the higher sequencing depth in Bd21 samples.

Focussing on 7980 single-copy orthogroups differentially expressed in both accessions, we found that fold-change values were strongly correlated between Bd21-3 and Bd21, suggesting a largely conserved transcriptional response to root tip excision (Fig. 2c; R^2_{adj} = 0.81, *P*-value < 0.001; Table S8). Among those differentially expressed single-copy orthogroups, we find that 583 and 1088 are consistently upregulated and downregulated in response to touch in *B. distachyon* roots, respectively, likely reflecting mechanical stimulation (Fig. S6; Coomey *et al.*, 2024) (Table S9). GO enrichment analysis of DEGs in both accessions revealed a strong overrepresentation of terms related to oxidoreductase and peroxidase activity (Fig. S7). In addition, we identified a set of 240 orthologs that exhibited inverse expression changes between Bd21 and Bd21-3 over the time course (Fig. 2c). GO enrichment analysis of these divergently regulated genes showed a significant enrichment for energy-intensive processes, such as Adenosine triphosphate hydrolysis (Fig. S8; Table S10). Further analysis of the top 100 most up- and downregulated genes in both accessions revealed consistent enrichment for cell wall-related enzymes, including glycosyl hydrolases, pectinesterases, and expansins. Notably, peroxidases exhibit the highest statistical enrichment among molecular function categories (Fig. 2d; False Discovery Rate (FDR) = 8.668000e-21 Fisher's exact test) (Table S11). In agreement, GO terms associated with carbohydrate metabolism and cell wall biogenesis were also significantly enriched at genes similarly differentially expressed in both accessions at early time points after root tip excision (Fig. 2e; Table S12).

To further explore the contribution of cell wall-related metabolism to lateral root emergence, we focussed on genes encoding proteins listed in the plant cell wall experimental database (Figs 2f, S9; Table S13). Approximately 87% of the expressed genes mapped to this database were differentially expressed after root tip excision (484 of 555 genes). Among the most deregulated protein families were peroxidases and proteins of unknown function. Several glycoside hydrolases (GHs) were also significantly misregulated following synchronization. Notably, 92% of the differentially expressed GH family 18 genes, which include chitinases, were upregulated after root tip excision (37 of 40). By contrast, 90% of the GH family 28 genes, which encode polygalacturonases involved in pectin remodelling, were downregulated together with many arabinogalactan proteins (30 of 33; Figs 2f, S9; Table S14). By contrast, pectin methylesterase and pectin methyltransferase inhibitors (61.5% and 90.9% upregulated respectively), expansin (70.5% upregulated), and glucan-acting glycosyl hydrolases (GH17, 77.5% upregulated), were predominantly upregulated. The differential regulation of these types of cell-wall-modifying enzymes in Bd21-3 might underly changes in the cell wall properties in the root tissue. Altogether, the transcriptomic analysis reveals that root tip excision triggers extensive cell wall remodelling in both *B. distachyon* accessions, with differences in timing, magnitude, and specific gene families likely underlying the difference between the 'pine tree' and the 'fishbone' phenotypes of lateral root emergence.

Differential lignification in the exodermis underlies the 'fishbone' root system architecture

To investigate potential differences in cell wall modifications following lateral root synchronization, we employed a histochemical approach to visualize major cell wall polymers. Given the strong enrichment of peroxidase-related GO terms in our transcriptomic data, we specifically examined lignin accumulation using phloroglucinol-HCl staining (Figs 3a, S10). At 40 h post excision, Bd21-3 roots exhibited stronger lignin staining along the root axis and vasculature compared to Bd21, suggesting greater overall lignin accumulation. To biochemically validate the visual increase in lignin content in Bd21-3 roots, we quantified total lignin content using the CASA method. This revealed no significant difference in control lignin levels (0 h) between the two accessions (Figs 3b, S11; Table S15). However, 40 h after root tip excision, Bd21-3 roots exhibited a significant increase in lignin content (18.71 ± 0.94%) compared to Bd21 (15.33 ± 0.50%, *P* = 0.0201).

To dissect the specific changes in lignin structure and content, we quantified monolignols using thioacidolysis. This revealed that Bd21-3 accumulated significantly higher levels of beta-O-4 linked H, G, and S units than Bd21, with a marked increase at 40 h after root tip excision. We find a more pronounced increase in monolignols in the upper part of the primary root after root tip post excision of Bd21-3 plants in which the number of lateral root emergence is decreased (Figs 3c, S12; Tables S16 and S17). Together, the chemical analyses confirm that in Bd21-3, the 'fishbone' phenotype is associated with a time-dependent and spatially defined increase in lignification. Focussing on the lignin biosynthetic pathway, we found that Bd21 and Bd21-3 differ in their transcriptomic response to lateral root synchronization

New Phytologist

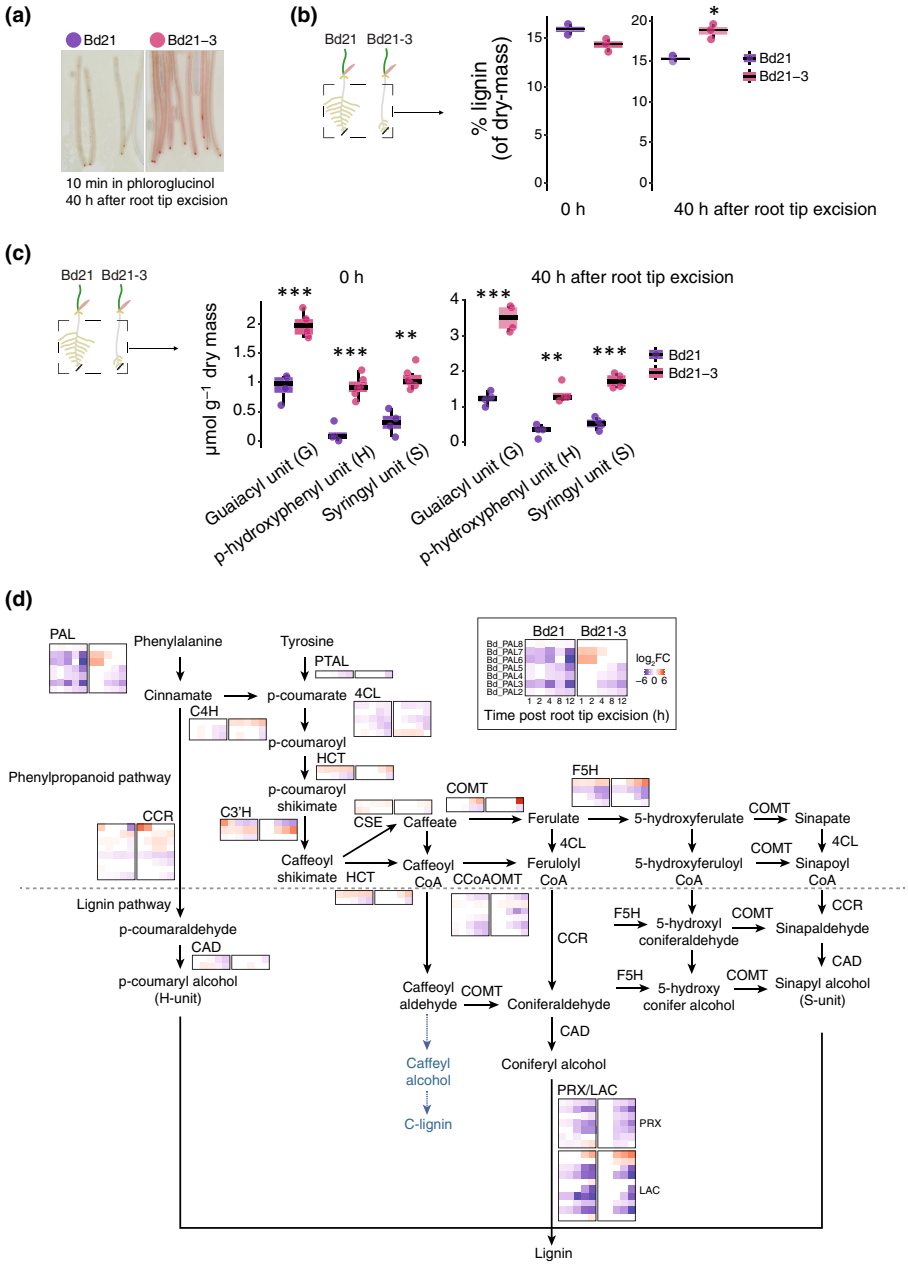

Fig. 3 Bd21-3 'fishbone' root phenotype correlates with increased lignin deposition and upregulated lignin biosynthesis following root tip excision. (a) Phloroglucinol-HCl staining of roots at 40 h after root tip excision reveals enhanced lignin accumulation in Bd21-3 compared to Bd21. Images are representative pooled individuals of three biological replicates. (b) Quantification of total lignin content by cysteine-assisted sulfuric acid in whole root systems at 0 and 40 h after root tip excision. (c) Thioacidolysis-based quantification of lignin monomer composition (µmol g^{-1} dry weight) in whole roots at 0 and 40 h after root tip excision, showing levels of guaiacyl (G), p-hydroxyphenyl (h), and syringyl (S) units. For each condition, roots from 30 to 50 seedlings were pooled per biological replicate ($n = 3$). In (b) and (c), each point represents a biological replicate. Statistical comparisons between genotypes at each time point were performed using two-sided Wilcoxon rank-sum tests (*, $P < 0.05$; **, $P < 0.01$; ***, $P < 0.001$). (d) Schematic overview of the phenylpropanoid and lignin biosynthesis pathways. Heatmaps show $\log_2$ fold changes in the expression of key biosynthetic genes at 1, 2, 4, 8, and 12 h after root tip excision in Bd21 and Bd21-3. For the boxplots, the central boxes represent the interquartile range, spanning the 25th (Q1) to the 75th percentile (Q3). The horizontal line inside each box indicates the median (50th percentile). Whiskers extend to the 5th and 95th percentiles, and individual points outside this range are shown as outliers.

(Fig. 3d; Table S18). In Bd21-3, *BdPHENYLALANINE AMMONIA-LYASE 6* (*BdPAL6*) and *BdPAL7*, which encode enzymes catalysing the deamination of phenylalanine in the first step of the phenylpropanoid pathway, were both upregulated after root tip excision. This was accompanied by the upregulation of *BdCINNAMATE-4-HYDROXYLASE 3*, indicating sustained flux through the lignin pathway. Further downstream, key genes involved in monolignol biosynthesis, including *Bd4-COUMARATE-COA LIGASE 1* and *BdCINNAMOYL-COA REDUCTASES 1–4*, showed higher fold-change in Bd21-3. Notably, induction of *BdCAFFEIC ACID O-METHYLTRANSFERASE 3* and *BdFERULATE 5-HYDROXYLASE 5* suggested further progression towards monolignol production. Analysis of MYELOBLASTOSIS (MYB) transcription factors, which act as upstream regulators of secondary cell wall biosynthesis, revealed that *BdMYB108* and *BdMYB112* homologs were consistently upregulated in Bd21-3, while *BdMYB54* and *BdMYB74* were upregulated and *BdMYB5* and *BdMYB50* downregulated in Bd21 (Fig. S13; Table S19). Altogether, these results indicate stronger transcriptional activation of lignin biosynthesis in Bd21-3 in response to root tip excision.

We then used Basic Fuchsin staining and confocal microscopy to achieve cellular resolution of the differential lignification. Confocal images show similar exodermis lignification patterns along the root tip-base axis in both accessions under normal conditions (Fig. S14). They also showed that, following root tip excision, basic fuchsin-stained lignification signals become stronger in both the proximal and distal regions relative to the root tip in both accessions (Figs S14 and S15). In addition, it also confirmed the exodermis as the site of the differential lignification between

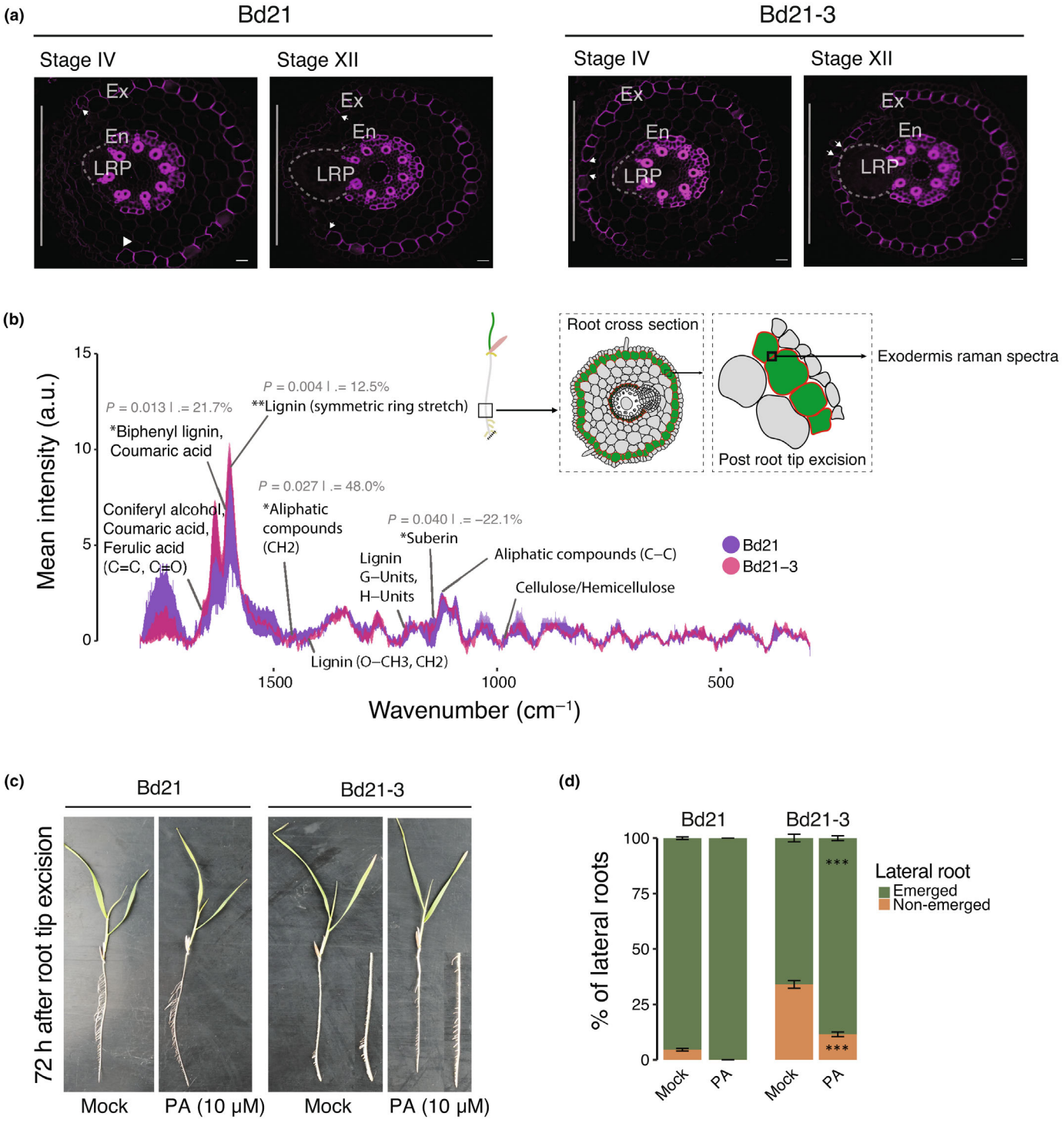

Fig. 4 Bd21-3 exhibits enhanced lignification of the exodermis during lateral root development following root tip excision. (a) Two-photon excitation microscopy images of Basic Fuchsin-stained root cross-sections from Bd21 (left panel) and Bd21-3 (right panel). A white vertical bar on the left side of each image marks the side facing the half-strength Murashige and Skoog medium. White arrowheads indicate the limits of exodermal lignification opposite the lateral root emergence side. Bars, 50 µm. Forty-five seedlings were analysed with three independent biological replicates for each staining approach. Ex, exodermis; En, endodermis; LRP, lateral root primordium. Bars, 20 µm. (b) Raman spectroscopy of the anticlinal cell walls of the exodermis region showing mean spectral intensities of major cell wall components in Bd21 and Bd21-3. Measurements were taken 40 h after root tip excision in the upper root region, targeting the exodermal anticlinal cell wall on the primordium-facing side. *p*-values and relative intensity changes are indicated. (c) Representative images of whole root systems of Bd21 and Bd21-3 seedlings 72 h after root tip excision treated with either mock or 10 µM piperonylic acid (PA). (d) Distribution of emerged and nonemerged lateral roots under mock and PA treatments. Bars show mean percentages (5–8 seedlings per condition, three biological replicates). Asterisks indicate significant differences between mock and PA treatment, assessed using a binomial generalized linear mixed model with seedling as the unit and Petri dish as a random effect. Error bars represent SE of the mean.

Bd21 and Bd21-3 (Fig. 4a). After root tip excision, exodermal lignification already appeared more intense during lateral root development in Bd21-3 compared with Bd21. By stage IV of lateral root development, the exodermis overlying the emergence zone in Bd21-3 appeared already fully lignified, creating a continuous barrier. This reinforcement correlated with a flattened morphology of the lateral root primordia, suggesting that exodermis lignification could promote a mechanical resistance to emergence (Fig. 4a). By contrast, exodermal lignification in Bd21 appeared less intense, allowing the lateral root to emerge with a typical elongated shape. Altogether, the lignin quantification and confocal microscopy show that enhanced lignification in Bd21-3 in the exodermis occurs earlier during lateral root development, potentially forming a physical barrier that delays emergence.

To gain precise *in situ* chemical insights, we performed confocal Raman spectroscopy 40 h after root tip excision in the upper root region, specifically targeting the exodermal anticlinal cell wall on the primordium-facing side, which showed the strongest Basic Fuchsin signal (Fig. 4b; Table S20). The resulting spectra revealed a profound chemical divergence between the two accessions. The exodermis of Bd21-3 exhibited significantly higher intensities for multiple peaks associated with lignin and phenolic compounds compared to Bd21. The most prominent lignin peak at *c.* 1600 cm^{-1} (symmetric ring stretch), a proxy for total lignin content, was 12.5% higher in Bd21-3 ($P = 0.004$). Furthermore, the peak at *c.* 1630 cm^{-1}, assigned to biphenyl lignin and coumaric acid, was 21.7% higher ($P = 0.013$). By contrast, a peak associated with suberin at *c.* 1125 cm^{-1} was significantly reduced by 22.1% in Bd21-3 ($P = 0.040$). This shift in chemical profile points to a divergent strategy in outer tissue reinforcement between accessions.

To functionally confirm that increased lignification participates in inhibiting lateral root emergence in Bd21-3, we applied PA, a chemical inhibitor of the lignin biosynthesis enzyme C4H (Lee *et al.*, 2013). Roots grown in the presence of PA for 60 h displayed markedly reduced lignin deposition in the exodermis (Ex) compared with mock-treated controls (Fig. S16). Cleared roots of mock-treated Bd21-3 plants displayed a significantly higher proportion of nonemerged lateral roots following root tip excision compared with Bd21. Treatment with PA (10 μM) markedly reduced this proportion in Bd21-3, restoring emergence levels closer to those observed in Bd21 (Fig. 4c,d; Table S21). By contrast, Bd21 plants maintained high levels of emergence under both mock and PA conditions. This corresponds to a partial, though incomplete, shift from the inhibited 'fishbone' root system architecture towards a more developed 'pine tree' phenotype, demonstrating that PA treatment partially rescues lateral root emergence in Bd21-3. Collectively, our results indicate that the Bd21-3 accession responds to root tip excision with a stress-induced response resulting in intense lignification in the exodermis, likely creating a rigid physical barrier that restricts lateral root emergence and alters overall root system architecture (Fig. 5).

Discussion

Here, we uncovered striking natural variation in Root System Architecture (RSA) plasticity in response to root tip excision between two *B. distachyon* accessions. We highlight two contrasting architectures, with Bd21 displaying a 'pine tree' phenotype marked by evenly spaced lateral roots along the primary root, while Bd21-3 exhibits a 'fishbone' phenotype in which lateral roots emerge proximally but with less numbers in the upper part of the primary root after root tip excision. Importantly, we show that the phenotypic divergence is not due to defects in lateral root initiation but rather to a block in emergence, specifically in the upper part of the primary root zone (Fig. 1).

Root tip excision has long been known to stimulate lateral roots formation and emergence across various plant species

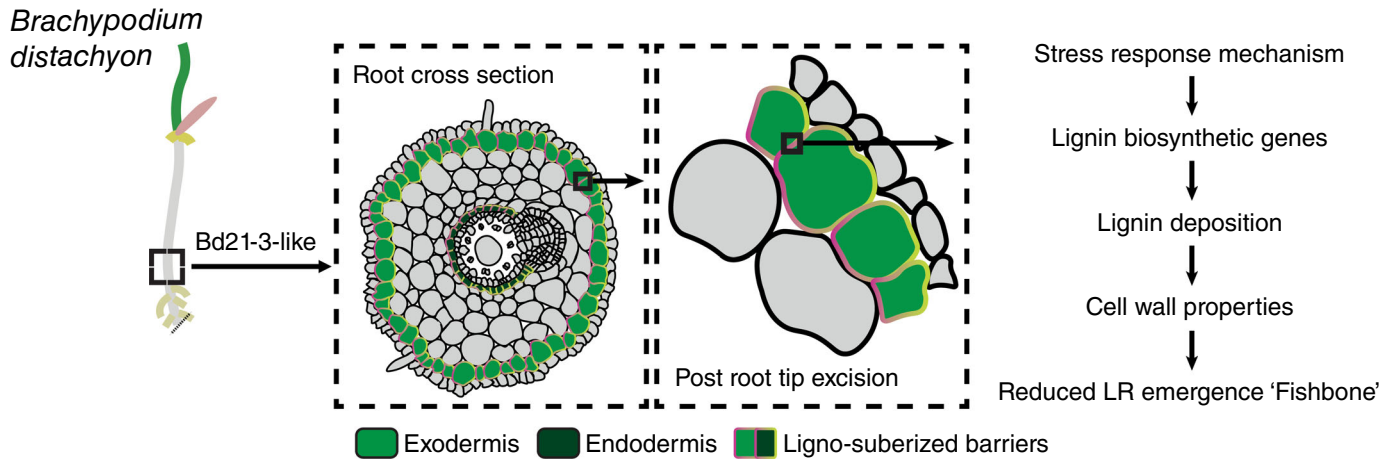

Fig. 5 Schematic model for the stress-induced inhibition of lateral root emergence in *Brachypodium distachyon* accession Bd21-3. This model illustrates the proposed mechanism underlying the 'fishbone' phenotype. A stress event, such as root tip excision, initiates a specific response pathway in the outer root tissues, particularly the exodermis. This response triggers the transcriptional activation of lignin biosynthetic genes, leading to increased lignin deposition within the exodermal cell walls. The resulting change in cell wall properties increases their rigidity, creating a mechanical constraint that ultimately causes delayed lateral root emergence.

(Torrey, 1950; Thomas *et al.*, 2014; Kawai *et al.*, 2017). In some cases, the differential emergence of lateral roots in proximal and upper regions may reflect differences in the developmental stage of lateral roots along the root axis. In rice, for instance, seminal root tip excision induces expansion of lateral root primordia through enhanced periclinal divisions in the ground tissue, but also a broader stele, and this response is most pronounced in lateral root primordia closest to the excision site (Kawai *et al.*, 2017). Furthermore, in rice, lateral root identity is defined by two distinct subtypes: long, highly branched L-type lateral roots and short, unbranched S-type lateral roots. Experiments involving root tip excision have shown that antagonistic interactions of *WUSCHEL-RELATED HOMEOBOX* transcription factors control the balance between L-type and S-type lateral roots, promoting the formation of L-type lateral roots while suppressing S-type lateral roots development (Kawai *et al.*, 2022). It would be valuable to explore whether *B. distachyon* also produces different lateral root types, *for example* L-type and S-type, and how their distribution varies along the primary root in relation to proximity to the excision site. The morphology and type of lateral roots could directly influence both the growth rate through overlying tissues and the timing of emergence. Thus, the pattern in lateral root emergence associated with the Bd21-3 'fishbone' phenotype may reflect not only changes in cell wall *that are* mechanical constraints but also differences in lateral root primordia identity and development.

Our results suggest that divergence in RSA could also arise, at least in part, from intraspecific genomic variation segregating among *B. distachyon* accessions, potentially contributing to local adaptation. Notably, differences in the expression of single-copy orthologous genes were observed during the later stages of the root tip excision response (Fig. 2a). Furthermore, GO enrichment analysis of genes within multicopy orthogroups specific to the Bd21 accession revealed a strong overrepresentation of BPs related to DNA repair and cellular responses to stress (Fig. S4). Bd21 may possess an expansion of stress-responsive gene families that enable more effective mitigation of cellular damage caused by wounding, facilitating a more developmentally permissive root program. Consistent with our observations, Kawai *et al.* (2022) also reported widespread differential expression of Domain of Unknown Function following root tip excision in rice, suggesting that members of this broad and poorly characterized gene family may play previously underappreciated roles in wound-induced transcriptional reprogramming. In *B. distachyon*, a pangenome built from 54 accessions showed that *c.* 65% of the gene pool is accessory, with many genes implicated in defence and development-related functions (Gordon *et al.*, 2017). This same pangenome revealed that gene presence/absence and copy number variation across accessions are tightly linked to population structure and adaptive traits. Further functional and population-level studies would help determine whether the two phenotypes are linked to adaptive strategies shaped by natural selection acting on the species' pangenome.

Our results highlighted pathway-wide reprogramming towards intensive lignin biosynthesis, both transcriptionally and biochemically. We find that following root tip excision, the root exodermis in the Bd21-3 accession accumulated significantly more lignin characterized by biphenyl 5–5′ cross-links derived primarily from guaiacyl (G) units (Boerjan *et al.*, 2003; Guadix-Montero & Sankar, 2018). The prevalence of G-units is known to promote a more cross-linked and condensed polymer structure, resulting in a stiffer, more recalcitrant matrix that can function as an effective physical barrier (Fig. 4b) (Rosado *et al.*, 2021; Balk *et al.*, 2023; Muretta *et al.*, 2024). Furthermore, under stress-like conditions, H-unit-rich lignin has been shown to accumulate (Tobimatsu & Schuetz, 2019; Gladala-Kostarz *et al.*, 2020). The increase in H-monomers observed in Bd21-3 likely reflects a similar cell wall stress response, triggered here by root tip excision. Although H-units are less commonly incorporated into developmental lignin, their presence is frequently associated with increased polymer rigidity and resistance to enzymatic degradation (Mamedes-Rodrigues *et al.*, 2019; Balk *et al.*, 2023). Notably, mechanical constraints resulting from this altered lignin composition have been linked to increased tissue brittleness, independent of total lignin quantity (Timpano *et al.*, 2015). These findings show that the spatial distribution and chemical composition of lignin influence the mechanical behaviour and developmental outcomes.

In our study, following root tip excision, these structural consequences are most apparent at the exodermis, in which Bd21-3 showed early and intense exodermal lignification directly above developing lateral roots, forming a continuous barrier (Fig. 4a). This lignified layer coincided with flattened, stalled primordia and a significant reduction in successful emergence events, *in fine* resulting morphologically as the 'fishbone' phenotype. Conversely, Bd21 displayed a more permissive response: Exodermal lignification was lower and localized, creating temporary openings that allowed lateral roots to emerge normally. Furthermore, the functional relevance of this mechanical barrier was further validated by pharmacological inhibition of lignin biosynthesis using PA, which partially allows lateral roots emergence and root architecture in Bd21-3 (Fig. 4c,d) following root tip excision. Together, our data support a model in which Bd21-3 activates a lignin-based fortification program in response to mechanical stress, characterized by early and localized deposition of G- and H-rich lignin polymers in the exodermis. Notably, the concurrent increase in S-units, typically associated with developmental lignin or hydrophobic sealing functions, suggests that both stress and developmental pathways may be co-opted in Bd21-3, possibly resulting in a lignin barrier that is both hydrophobic and mechanically rigid (Vanholme *et al.*, 2012; Barros *et al.*, 2015). The reinforcement of the outer root tissues in Bd21-3 likely impacts the flexibility needed to accommodate lateral root emergence. In *A. thaliana*, compromised Casparian strip integrity and low calcium availability promote ectopic lignin deposition in the endodermis in a SGN3/GSO1-dependent manner (Lai *et al.*, 2025). This excessive barrier lignification mechanically impedes lateral root emergence, defining a developmental checkpoint in which lignin functions as a mechanical gatekeeper (Banda *et al.*, 2019). In Bd21-3, local lignification of the exodermis is strongly induced as a protective response to wounding and similarly acts as a mechanical constraint on organ emergence.

Whether a surveillance system is actively involved in the balance between organogenesis and the response to wounding in both accessions remains unknown.

Other plant species have shown similar plasticity of their root exodermis cell layer. In tomato (*Solanum lycopersicum*), the exodermis does not form a Casparian strip but instead develops a structurally distinct polar lignin cap that functions as a selective apoplastic barrier (Manzano *et al.*, 2024). Although functionally analogous to the endodermal Casparian strip, the regulation of this polar lignin cap involves a genetically distinct module, and its formation is spatially restricted to the outermost cortical layer by the repressive action of the transcription factors *SlSCHIZORIZA* (*SlSCZ*) and *SlEXO1*. Observations on different plant species therefore suggest a form of functional convergence, in which lignin-based barriers with comparable physiological roles can emerge through unique regulatory pathways. In addition to the lignified barrier, exodermis suberization is also critical for drought tolerance in tomato, operating as a functional equivalent to the *A. thaliana* endodermis (Manzano *et al.*, 2024). In tomato, the conserved suberin biosynthetic pathway, including regulators like *SlMYB92*, has been evolutionarily rewired to act in the exodermis rather than the endodermis (Cantó-Pastor *et al.*, 2024). Recently, abscisic acis (ABA) was shown to first activate general stress-responsive elements and then induce lignin and suberin biosynthesis through MYB transcription factors in chickpea (Jo *et al.*, 2025). In our dataset, several MYB genes known to be ABA-responsive, such as *MYB94*, *MYB91*, *MYB108*, and *MYB112*, were constitutively upregulated in Bd21-3, while others such as *MYB93*, a negative regulator of lateral root emergence (Xiao *et al.*, 2021; Uemura *et al.*, 2023), were downregulated. These patterns would point to ABA as a key upstream regulator of the altered MYB landscape in Bd21-3.

In *A. thaliana*, cell wall remodelling plays a central role in lateral root emergence (Swarup *et al.*, 2008; Péret *et al.*, 2012; Kumpf *et al.*, 2013; Lewis *et al.*, 2013; Lucas *et al.*, 2013; Roycewicz & Malamy, 2014; Vermeer *et al.*, 2014; Berhin *et al.*, 2019;Wachsman *et al.*, 2020; Ursache *et al.*, 2021). Consistent with this, our time-course transcriptomic analysis revealed dynamic regulation of numerous cell-wall-modifying enzyme families, particularly GHs, in both *B. distachyon* accessions after root tip excision (Figs 2d–f, S7–S9). This suggests a tightly orchestrated remodelling process, potentially involving both cell wall loosening and reinforcement in a spatially and temporally regulated manner across different tissue layers. Recent studies have underscored that lateral root emergence depends on precise and layer-specific remodelling of the cell wall (Wachsman *et al.*, 2020; Ursache *et al.*, 2021). A key future challenge will be to integrate single-cell transcriptomics with high-resolution cell wall chemical profiling, enabling the mapping of transcriptional programs directly to physical changes in tissue properties. Moreover, genome-wide association studies across diverse *B. distachyon* accessions could help pinpoint the genetic loci responsible for variation in the root system architecture. In conclusion, our study reveals that, in response to wounding, exodermal lignification acts as a dynamically regulated mechanical barrier that can restrict lateral root emergence, driving intraspecific variation in the overall RSA. Far from being a passive structural layer, the exodermis emerges as a key regulatory interface, responsive to both intrinsic developmental signals and extrinsic stress cues. These findings not only advance our understanding of root development in grasses but also open promising avenues for engineering stress-resilient crops by targeting the regulatory pathways that govern root barrier plasticity.

Acknowledgements

We thank the three anonymous reviewers and the editor for their constructive feedback on the manuscript. We also would like to thank the Botanical Garden of Neuchâtel and the University of Neuchâtel for their support in propagating and maintaining the *Brachypodium distachyon* accessions collection. Parts of the text were improved in flow and clarity with assistance from ChatGPT. KB was supported by a Marie Skłodowska-Curie Global Fellowship (PLANTiD, Grant Agreement No. 101106663). Work in the Vermeer lab was funded by the Swiss National Science Foundation (project nos.: 157524, 197568 and 231162 awarded to JEMV) and by the University of Neuchâtel. Open access publishing facilitated by Universite de Neuchatel, as part of the Wiley - Universite de Neuchatel agreement via the Consortium Of Swiss Academic Libraries.

Competing interests

None declared.

Author contributions

CDJVT and KB characterized the root system architecture phenotypes in *Brachypodium distachyon* accessions. ACR provided the Mediterranean *B. distachyon* accessions. CDJVT and KB generated the seed resources for these accessions, with support from the Botanical Garden of Neuchâtel. CDJVT prepared the RNA samples with assistance from KB. TB performed the genomic analyses and processed the transcriptomic data. LP, RS, and KB conducted lignin quantification. AO and KB carried out the Raman spectroscopy analysis. CDJVT and KB performed the brightfield and confocal imaging. MM performed the experiments with Basic Fuchsin to visualize changes in lignification. KB, TB and JEMV conceived and designed the research. TB prepared the figures with input from KB. KB and TB cowrote the first draft of the manuscript. KB, TB and JEMV supervised the project.

ORCID

Thomas Badet https://orcid.org/0000-0001-6130-441X
Kevin Bellande https://orcid.org/0000-0003-0478-2567
Angelina D'Orlando https://orcid.org/0000-0002-8118-3819
Marius Malai https://orcid.org/0000-0003-3424-9560
Anne C. Roulin https://orcid.org/0000-0002-6668-3321

Richard Sibout https://orcid.org/0000-0002-0639-5643
Joop E. M. Vermeer https://orcid.org/0000-0001-8876-5873
Cristovão De Jesus Vieira Teixeira https://orcid.org/0000-0003-3984-5513

Data availability

The data that support this study are available within the article as part of the Tables S1–S21. The RNA-sequencing raw sequencing data were deposited at the NCBI Short Read Archive under the accession no. PRJNA1312106.

References

Anders S, Pyl PT, Huber W. 2015. HTSeq—a Python framework to work with high-throughput sequencing data. *Bioinformatics* **31**: 166–169.

Artur MA, Kajala K, Mariana S, Artur CA. 2021. Convergent evolution of gene regulatory networks underlying plant adaptations to dry environments. *Plant, Cell & Environment* **44**: 3211–3222.

Balk M, Sofia P, Neffe AT, Tirelli N. 2023. Lignin, the lignification process, and advanced, lignin-based materials. *International Journal of Molecular Sciences* **24**: 11668.

Banda J, Bellande K, von Wangenheim D, Goh T, Guyomarc'h S, Laplaze L, Bennett MJ. 2019. Lateral root formation in Arabidopsis: a well-ordered LRexit. *Trends in Plant Science* **24**: 826–839.

Barros J, Serk H, Granlund I, Pesquet E. 2015. The cell biology of lignification in higher plants. *Annals of Botany* **115**: 1053–1074.

Beckers A, Mamiya A, Furutani M, Bennett MJ, Fukaki H, Sawa S, Gantet P, Laplaze L, Guyomarc'h S. 2024. Multiple layers of regulators emerge in the network controlling lateral root organogenesis. *Trends in Plant Science* **30**: 499–514.

Berhin A, de Bellis D, Franke RB, Buono RA, Nowack MK, Nawrath C. 2019. The root cap cuticle: a cell wall structure for seedling establishment and lateral root formation. *Cell* **176**: 1367–1378.e8.

Boerjan W, Ralph J, Baucher M. 2003. Lignin biosynthesis. *Annual Review of Plant Biology* **54**: 519–546.

Bushnell B. 2014. BBMap: A Fast, Accurate, Splice-Aware Aligner. Report Number: LBNL-7065E, Lawrence Berkeley National Laboratory, Berkeley, CA, USA. [WWW document] URL https://sourceforge.net/projects/bbmap/

Cantó-Pastor A, Kajala K, Shaar-Moshe L, Manzano C, Timilsena P, De Bellis D, Gray S, Holbein J, Yang H, Mohammad S *et al.* 2024. A suberized exodermis is required for tomato drought tolerance. *Nature Plants* **10**: 118–130.

Chochois V, Voge JP, Rebetzke GJ, Watt M. 2015. Variation in adult plant phenotypes and partitioning among seed and stem-borne roots across *Brachypodium distachyon* accessions to exploit in breeding cereals for well-watered and drought environments. *Plant Physiology* **168**: 953–967.

Coomey JH, Mackinnon KJM, Mccahill IW, Khahani B, Handakumbura PP, Trabucco GM, Mazzola J, Leblanc NA, Kheam R, Hernandez-Romero M *et al.* 2024. Mechanically induced localisation of SECONDARY WALL INTERACTING bZIP is associated with thigmomorphogenic and secondary cell wall gene expression. *Quantitative Plant Biology* **5**: e5.

Diehn S, Kirby N, Ben-Zeev S, Alemu MD, Saranga Y, Elbaum R. 2024. Raman developmental markers in root cell walls are associated with lodging tendency in tef. *Planta* **259**: 54.

Dobin A, Davis CA, Schlesinger F, Drenkow J, Zaleski C, Jha S, Batut P, Chaisson M, Gingeras TR. 2013. STAR: ultrafast universal RNA-seq aligner. *Bioinformatics* **29**: 15–21.

Emms DM, Kelly S. 2019. OrthoFinder: phylogenetic orthology inference for comparative genomics. *Genome Biology* **20**: 1–14.

Filiz E, Ozdemir BS, Budak F, Vogel JP, Tuna M, Budak H. 2009. Molecular, morphological, and cytological analysis of diverse *Brachypodium distachyon* inbred lines. *Genome* **52**: 876–890.

Geldner N. 2013. The endodermis. *Annual Review of Plant Biology* **64**: 531–558.

Gladala-Kostarz A, Doonan JH, Bosch M. 2020. Mechanical stimulation in *Brachypodium distachyon*: implications for fitness, productivity, and cell wall properties. *Plant, Cell & Environment* **43**: 1314–1330.

González JM, Redondo-Pedraza J, Loarce Y, Hammami R, Friero E, Jouve N. 2020. Molecular genetic analysis of drought stress response traits in Brachypodium spp. *Agronomy* **10**: 518.

Gordon SP, Contreras-Moreira B, Woods DP, Des Marais DL, Burgess D, Shu S, Stritt C, Roulin AC, Schackwitz W, Tyler L *et al.* 2017. Extensive gene content variation in the *Brachypodium distachyon* pan-genome correlates with population structure. *Nature Communications* **8**: 1–13.

Guadix-Montero S, Sankar M. 2018. Review on catalytic cleavage of C–C inter-unit linkages in lignin model compounds: towards lignin depolymerisation. *Topics in Catalysis* **61**: 183–198.

Höfte H, Voxeur A. 2017. Plant cell walls. *Current Biology: CB* **27**: R865–R870.

Ingram PA, Zhu J, Shariff A, Davis IW, Benfey PN, Elich T. 2012. High-throughput imaging and analysis of root system architecture in *Brachypodium distachyon* under differential nutrient availability. *Philosophical Transactions of the Royal Society, B: Biological Sciences* **367**: 1559–1569.

de Jesus Vieira Teixeira C, Bellande K, van der Schuren A, O'Connor D, Hardtke CS, Vermeer JEM. 2024. An atlas of *Brachypodium distachyon* lateral root development. *Biology Open* **13**: bio060531.

Jo L, Kluck R, Buti S, Holbein J, Chhillar H, Ding P, Franke RB, Kajala K. 2025. ABA-induced MYB transcriptional module regulates the differentiation trajectory of chickpea exodermis. *bioRxiv*. doi: 10.1101/2025.01.03.631192.

Kawai T, Nosaka-Takahashi M, Yamauchi A, Inukai Y. 2017. Compensatory growth of lateral roots responding to excision of seminal root tip in rice. *Plant Roots* **11**: 48–57.

Kawai T, Shibata K, Akahoshi R, Nishiuchi S, Takahashi H, Nakazono M, Kojima T, Nosaka-Takahashi M, Sato Y, Toyoda A *et al.* 2022. WUSCHEL-related homeobox family genes in rice control lateral root primordium size. *Proceedings of the National Academy of Sciences, USA* **119**: e2101846119.

Kumpf RP, Shi CL, Larrieu A, Stø IM, Butenko MA, Péret B, Riiser ES, Bennett MJ, Aalen RB. 2013. Floral organ abscission peptide IDA and its HAE/HSL2 receptors control cell separation during lateral root emergence. *Proceedings of the National Academy of Sciences, USA* **110**: 5235–5240.

Lai Y, Feng Z, Lin X, Shi W, Busch W, Li B. 2025. Endodermal lignification coordinates with root calcium levels to govern lateral root emergence. *New Phytologist* **247**: 1290–1307.

Lapierre C, Rolando C. 1988. Thioacidolyses of pre-methylated lignin samples from pine compression and poplar woods. *Holzforschung* **42**: 1–4.

Lee Y, Rubio MC, Alassimone J, Geldner N. 2013. A mechanism for localized lignin deposition in the endodermis. *Cell* **153**: 402–412.

Lewis DR, Olex AL, Lundy SR, Turkett WH, Fetrow JS, Muday GK. 2013. A kinetic analysis of the auxin transcriptome reveals cell wall remodeling proteins that modulate lateral root development in Arabidopsis. *Plant Cell* **25**: 3329–3346.

Li H, Handsaker B, Wysoker A, Fennell T, Ruan J, Homer N, Marth G, Abecasis G, Durbin R. 2009. The sequence Alignment/Map format and SAMtools. *Bioinformatics* **25**: 2078–2079.

Liu T, Kreszies T. 2023. The exodermis: a forgotten but promising apoplastic barrier. *Journal of Plant Physiology* **290**: 154118.

Love MI, Huber W, Anders S. 2014. Moderated estimation of fold change and dispersion for RNA-seq data with DESeq2. *Genome Biology* **15**: 1–21.

Lucas M, Kenobi K, Wangenheim D, Voβ U, Swarup K, De SI, Van DD, Lawrence T, Péret B, Moscardi E *et al.* 2013. Lateral root morphogenesis is dependent on the mechanical properties of the overlaying tissues. *Proceedings of the National Academy of Sciences, USA* **110**: 5229–5234.

Ludwig E, Sumner J, Berry J, Polydore S, Ficor T, Agnew E, Haines K, Greenham K, Fahlgren N, Mockler TC *et al.* 2024. Natural variation in *Brachypodium distachyon* responses to combined abiotic stresses. *The Plant Journal* **117**: 1676–1701.

Luo N, Liu J, Yu X, Jiang Y. 2011. Natural variation of drought response in *Brachypodium distachyon*. *Physiologia Plantarum* **141**: 19–29.

Lynch J, Zappala S, Tracy SR, Sturrock C, Bennett M, Mooney SJ, Pridmore T. 1995. Root architecture and plant productivity. *Plant Physiology* **109**: 7–13.

Lynch JP. 2019. Root phenotypes for improved nutrient capture: an underexploited opportunity for global agriculture. *New Phytologist* **223**: 548–564.

Mamedes-Rodrigues TC, Batista DS, Napoleão TA, Fortini EA, Cruz ACF, Costa MGC, Otoni WC. 2019. Regulation of cell wall development in *Brachypodium distachyon in vitro* as affected by cytokinin and gas exchange. *Plant Cell, Tissue and Organ Culture* **136**: 207–219.

Manzano C, Morimoto KW, Shaar-Moshe L, Mason GA, Cantó-Pastor A, Gouran M, De Bellis D, Ursache R, Kajala K, Sinha N *et al.* 2024. Regulation and function of a polarly localized lignin barrier in the exodermis. *Nature Plants* **2024**: 1–13.

Maqbool S, Hassan MA, Xia X, York LM, Rasheed A, He Z. 2022. Root system architecture in cereals: progress, challenges and perspective. *The Plant Journal* **110**: 23–42.

Muretta JE, Uriarte J, Compton D, LaDouceur R, Kirtley J, Prieto-Centurion D. 2024. Effects of lignin syringyl to guaiacyl ratio on cottonwood biochar adsorbent properties and performance. *Scientific Reports* **14**: 1–13.

Pacheco-Villalobos D, Sankar M, Ljung K, Hardtke CS. 2013. Disturbed local auxin homeostasis enhances cellular anisotropy and reveals alternative wiring of auxin-ethylene crosstalk in *Brachypodium distachyon* seminal roots. *PLoS Genetics* **9**: e1003564.

Pende M, Pende M, Vadiwala K, Schmidbaur H, Stockinger AW, Murawala P, Saghafi S, Dekens MPS, Becker K, Becker K *et al.* 2020. A versatile depigmentation, clearing, and labeling method for exploring nervous system diversity. *Science Advances* **6**: eaba0365.

Péret B, Li G, Zhao J, Band LR, Voß U, Postaire O, Luu DT, Da Ines O, Casimiro I, Lucas M *et al.* 2012. Auxin regulates aquaporin function to facilitate lateral root emergence. *Nature Cell Biology* **14**: 991–998.

Pertea M, Pertea G. 2020. GFF utilities: GffRead and GffCompare. *F1000Research* **9**: 304.

Petrova A, Ageeva M, Kozlova L. 2023. Root growth of monocotyledons and dicotyledons is limited by different tissues. *The Plant Journal* **116**: 1462–1476.

R Project R: The R Project for Statistical Computing.

Ramachandran P, Ramirez A, Dinneny JR. 2024. Rooting for survival: how plants tackle a challenging environment through a diversity of root forms and functions. *Plant Physiology* **197**: 586.

Rice P, Longden L, Bleasby A. 2000. EMBOSS: The European Molecular Biology Open Software Suite. *Trends in Genetics* **16**: 276–277.

Rosado MJ, Rencoret J, Marques G, Gutiérrez A, del Río JC. 2021. Structural characteristics of the guaiacyl-rich lignins from rice (*Oryza sativa* L.) Husks and Straw. *Frontiers in Plant Science* **12**: 640475.

Rouina H, Singh D, Arlt C, Malekian B, Schreiber L, Stich B, Marshall-Colon A. 2025. Regulatory analysis of root architectural and anatomical adaptation to nitrate and ammonium in *Brachypodium distachyon. bioRxiv.* https://doi.org/10.1101/2025.01.06.631519.

Roycewicz PS, Malamy JE. 2014. Cell wall properties play an important role in the emergence of lateral root primordia from the parent root. *Journal of Experimental Botany* **65**: 2057–2069.

Sarkar P, Bosneaga E, Auer M. 2009. Plant cell walls throughout evolution: towards a molecular understanding of their design principles. *Journal of Experimental Botany* **60**: 3615–3635.

Schwartz CJ, Doyle MR, Manzaneda AJ, Rey PJ, Mitchell-Olds T, Amasino RM. 2010. Natural variation of flowering time and vernalization responsiveness in *Brachypodium distachyon. Bioenergy Research* **3**: 38–46.

Shang E, Tu Q, Yu Z, Ding Z. 2025. Cell wall dynamic changes and signaling during plant lateral root development. *Journal of Integrative Plant Biology* **67**: 632–648.

Smith S, de Smet I. 2012. Root system architecture: insights from Arabidopsis and cereal crops. *Philosophical Transactions of the Royal Society, B: Biological Sciences* **367**: 1441–1452.

Stoeckle D, Thellmann M, Vermeer JE. 2018. Breakout—lateral root emergence in Arabidopsis thaliana. *Current Opinion in Plant Biology* **41**: 67–72.

Stritt C, Gimmi EL, Wyler M, Bakali AH, Skalska A, Hasterok R, Mur LAJ, Pecchioni N, Roulin AC. 2022. Migration without interbreeding: evolutionary history of a highly selfing Mediterranean grass inferred from whole genomes. *Molecular Ecology* **31**: 70–85.

Swarup K, Benková E, Swarup R, Casimiro I, Péret B, Yang Y, Parry G, Nielsen E, De Smet I, Vanneste S *et al.* 2008. The auxin influx carrier LAX3 promotes lateral root emergence. *Nature Cell Biology* **10**: 946–954.

Thomas S, Sreelakshmi Y, Sharma R. 2014. Light modulates the root tip excision induced lateral root formation in tomato. *Plant Signaling & Behavior* **9**: e970098.

Timpano H, Sibout R, Devaux MF, Alvarado C, Looten R, Falourd X, Pontoire B, Martin M, Legée F, Cézard L *et al.* 2015. Brachypodium cell wall mutant with enhanced saccharification potential despite increased lignin content. *Bioenergy Research* **8**: 53–67.

Tobimatsu Y, Schuetz M. 2019. Lignin polymerization: how do plants manage the chemistry so well? *Current Opinion in Biotechnology* **56**: 75–81.

Torrey JG. 1950. The induction of lateral roots by indoleacetic acid and root decapitation. *American Journal of Botany* **37**: 257–264.

Uemura Y, Kimura S, Ohta T, Suzuki T, Mase K, Kato H, Sakaoka S, Uefune M, Komine Y, Hotta K *et al.* 2023. A very long chain fatty acid responsive transcription factor, MYB93, regulates lateral root development in Arabidopsis. *The Plant Journal* **115**: 1408–1427.

Ursache R, De Jesus Vieira Teixeira C, Dénervaud Tendon V, Gully K, De Bellis D, Schmid-Siegert E, Grube Andersen T, Shekhar V, Calderon S, Pradervand S *et al.* 2021. GDSL-domain proteins have key roles in suberin polymerization and degradation. *Nature Plants* **7**: 353–364.

Vadodaria R, Anderson CT. 2025. Branching under pressure: influences of cell wall architecture and biomechanics on lateral root morphogenesis. *Current Opinion in Plant Biology* **85**: 102735.

Vanholme R, Morreel K, Darrah C, Oyarce P, Grabber JH, Ralph J, Boerjan W. 2012. Metabolic engineering of novel lignin in biomass crops. *New Phytologist* **196**: 978–1000.

Vermeer JEM, von Wangenheim D, Barberon M, Lee Y, Stelzer EHK, Maizel A, Geldner N. 2014. A spatial accommodation by neighboring cells is required for organ initiation in Arabidopsis. *Science* **343**: 178–183.

Voxeur A, Wang Y, Sibout R. 2015. Lignification: different mechanisms for a versatile polymer. *Current Opinion in Plant Biology* **23**: 83–90.

Wachsman G, Zhang J, Moreno-Risueno MA, Anderson CT, Benfey PN. 2020. Cell wall remodeling and vesicle trafficking mediate the root clock in Arabidopsis. *Science* **370**: 819–823.

Xiao R, Zhang C, Guo X, Li H, Lu H. 2021. MYB transcription factors and its regulation in secondary cell wall formation and lignin biosynthesis during xylem development. *International Journal of Molecular Sciences* **22**: 3560.

Zhu M, Hsu CW, Peralta Ogorek LL, Taylor IW, La Cavera S, Oliveira DM, Verma L, Mehra P, Mijar M, Sadanandom A *et al.* 2025. Single-cell transcriptomics reveal how root tissues adapt to soil stress. *Nature* **642**: 721–729.

Supporting Information

Additional Supporting Information may be found online in the Supporting Information section at the end of the article.

Fig. S1 Bd21 and Bd21-3 display distinct lateral root emergence dynamics following root tip excision.

Fig. S2 Lateral root primordium development is synchronized and comparable between accessions.

Fig. S3 Bd21 'pine-tree' and Bd21-3 'fishbone' root phenotypes 60 h after root tip excision.

Fig. S4 Orthogroups with multiple copies in the Bd21 accession are enriched for stress and DNA repair functions.

Fig. S5 RNA-seq analysis highlights distinct early and late transcriptional responses in both *B. distachyon* accessions.

Fig. S6 Number of responsive genes to mechanical stimulation (touch) and root tip excision in *B. distachyon* roots.

Fig. S7 Molecular function gene ontology enrichment of deregulated genes in both Bd21 and Bd21-3 in response to root tip excision.

Fig. S8 Gene Ontology enrichment analysis for differentially expressed genes.

Fig. S9 Comparative transcriptomic analysis reveals a divergent cell wall remodelling response in Bd21 and Bd21-3 after root tip excision.

Fig. S10 Spatio-temporal analysis of lignin deposition after root tip excision.

Fig. S11 Increased lignin deposition following root tip excision in Bd21-3.

Fig. S12 Lignin monomer composition is elevated in the upper root zone of Bd21-3.

Fig. S13 Expression dynamics of selected MYB transcription factor homologs following root tip excision.

Fig. S14 Bd21 and Bd21-3 show similar exodermis lignification patterns along the root tip–base axis.

Fig. S15 Accession-specific patterns of exodermis lignification during lateral root emergence.

Fig. S16 Reduced exodermal lignin accumulation in Brachypodium roots following piperonylic acid (PA) treatment.

Table S1 Root phenotyping data for *B. distachyon* accessions.

Table S2 Root length data for *B. distachyon* accessions.

Table S3 Number of emerged lateral roots after root tip excision.

Table S4 Proportions of lateral root primordia stages in the primary root at in different zones after root tip excision.

Table S5 Number of emerged lateral roots after root-tip excision.

Table S6 Orthology assignment between Bd21 and Bd21-3 proteins as per orthofinder output.

Table S7 Summary table of the differential gene expression analysis performed using DESeq2 across multiple time points following root tip excision, relative to the baseline (0 h).

Table S8 Comparison of differential gene expression for single-copy orthologs between the two *B. distachyon* accessions across multiple time points following root tip excision.

Table S9 Differentially expressed genes in both, our root tip excision and the root touch experiment from Coomey *et al.* (2024).

Table S10 Gene ontology enrichment at the molecular function level of differentially expressed genes.

Table S11 Summary of word occurrences in the Pfam description of the top 100 up- and downregulated genes in the full transcriptomic dataset.

Table S12 Gene ontology enrichment at the biological process level of genes similarly differentially expressed in both accessions.

Table S13 Differential expression of a selection of cell-wall-related enzyme families and their functional annotation in the WallProt database.

Table S14 Differential expression of cell wall-related gene families.

Table S15 Quantification of total lignin content by CASA in whole root systems at 0 and 40 h after root tip excision.

Table S16 Quantification of total lignin content by thioacidolysis in the primary roots at 0 and 40 h after root tip excision.

Table S17 Quantification of total lignin content by thioacidolysis in specific zones of the primary roots at 0 and 40 h after root tip excision.

Table S18 Differential expression of lignin biosynthesis-related genes.

Table S19 Differential expression of MYB-related transcriptional factor genes.

Table S20 Summary statistics of the RAMAN spectra at the cell-walls of the root exodermis.

Table S21 Proportions of emerged vs non-emerged lateral root for Bd21 and Bd21-3 seedlings treated with either mock solution or 10 μM piperonylic acid (PA).

Please note: Wiley is not responsible for the content or functionality of any Supporting Information supplied by the authors. Any queries (other than missing material) should be directed to the *New Phytologist* Central Office.